Influence of the capillaries bed in hyperthermia for cancer treatment

Antônio Marchese Bravo Esteves[1][0000−0001−5130−4221], Gustavo Resende Fatigate[2][0000−0002−2600−2974], Marcelo Lobosco[1,2][0000−0002−7205−9509], and Ruy Freitas Reis[1,2⋆][0000−0001−5215−3744]

[1] Departamento de Ciência da Computação, Universidade Federal de Juiz de Fora, Brazil
[2] Pós-Graduação em Modelagem Computacional, Universidade Federal de Juiz de Fora, Brazil
ruy.reis@ufjf.br

Abstract. This work presents the computational modeling of solid tumor treatments with hyperthermia using magnetic nanoparticles, considering a bioheat transfer model proposed by Pennes(1948). The simulations consider a tumor seated in a muscle layer. The model was described with a partial differential equation, and its solution was approximated using the finite difference method in a heterogeneous porous medium using a Forward Time Centered Space scheme. Moreover, the Monte Carlo method was employed to quantify the uncertainties of the quantities of interest (QoI) considered in the simulations. The QoI considers uncertainties in three different parameters: 1) the angulation of blood vessels, 2) the magnitude of blood flow, and 3) the number of blood vessels per tissue unit. Since Monte Carlo demands several executions of the model and solving a partial differential equation in a bi-dimensional domain demands significant computational time, we use the OpenMP parallel programming API to speed up the simulations. The results of the in silico experiments showed that considering the uncertainties presented in the three parameters studied, it is possible to plan hyperthermia treatment to ensure that the entire tumor area reaches the target temperature that leads to damage.

Keywords: Hyperthermia · Cancer · Bioheat · Uncertainty Quantification · Monte Carlo

1 Introduction

Cancer is the name given to a large group of diseases that can start in almost any organ or tissue in the body. According to the World Health Organization [34], cancer is a leading cause of death worldwide: about 10 million deaths in 2020 were due to cancer. The leading causes of new cases of cancer in 2020 were breast (2.26 million cases), lung (2.21 million cases), colon and rectum (1.93

⋆ corresponding author

ICCS Camera Ready Version 2023
To cite this paper please use the final published version:
DOI: 10.1007/978-3-031-36021-3_60

million cases), prostate (1.41 million cases), skin (non-melanoma) (1.20 million cases), and stomach (1.09 million cases). On the other hand, the leading causes of death due cancer in the same year were lung (1.80 million deaths), colon and rectum (916,000 deaths), liver (830,000 deaths), stomach (769,000 deaths), and breast (685,000 deaths) [34].

A correct cancer diagnosis is essential for appropriate and effective treatment because every cancer type requires a specific treatment regimen. In recent years several methods have been developed to fight cancer. The most common treatments are surgery, radiotherapy, and systemic therapy (chemotherapy, hormonal treatments, targeted biological therapies) [20].

One of the treatments that have been studied against cancer is hyperthermia. Hyperthermia was discovered in the 1950s [5], and since then, it has been gaining space as a possible cancer treatment. The main idea behind this treatment is to superheat the tissue to a temperature threshold that induces cell necrosis [17]. Thus, it is possible to destroy tumor cells without a surgical procedure. Currently, hyperthermia is used as a non-invasive therapy against cancer, helping other techniques such as chemotherapy and radiotherapy [6, 17]. The hyperthermia is widely used in the treatment of liver [16] and breast tumors [9].

One of the ways to carry out the treatment through hyperthermia is with the application of magnetic nanoparticles [18, 19]. Nanoparticles can be applied to irregular and deep tumor tissues, and when exposed to a low-frequency alternating magnetic field, they overheat the site. Most of the heat generated by these nanoparticles is due to Néelian, and Brownian relaxation [18, 27]

Despite being discovered in the 50s [5], hyperthermia as a cancer treatment is still in an early stage of development, with open questions that can be answered with the help of mathematical models and computational simulations. Mathematical models were developed and applied to describe the heat in living tissues [12, 13, 21, 24, 25]. In this paper, a mathematical model described using partial differential equations (PDEs) is employed to describe the heat dynamics over time due to hyperthermia treatment. A porous media approach [13] is used to describe bioheat according to the properties of the living tissue, such as porosity, density, specific heat, thermal conductivity, metabolism, and velocity field.

The solution of PDEs is still a great challenge for science and engineering once most differential equations do not have an analytical solution. So, these models use numerical methods to solve them. This work employs the explicit Euler's method and the finite difference method (FDM) in a porous heterogeneous medium using a Forward Time Centered Space (FTCS) scheme to solve the mathematical model numerically.

Uncertainties are intrinsic to nature. Uncertainty quantification (UQ) is used to determine the likely results of models with stochastic behavior [7]. This paper uses Monte Carlo (MC) to include stochastic behavior for the UQ [28]. The deterministic model is solved several times, considering the uncertainties in some parameters. In our model, the uncertainties associated with several parameters, such as the number of blood capillaries, the magnitude, and the direction of

ICCS Camera Ready Version 2023
To cite this paper please use the final published version:
DOI: 10.1007/978-3-031-36021-3_60

blood velocity, are described as a density probability function (PDF) based on parameters found in the literature. We consider that both the blood capillaries and their associated values have a stochastic behavior because cancer growth can stimulate the capillaries' angiogenesis in the tumor site [8, 37]. Also, they depend on the cancer type, stage, location, and other specificities [11, 37].

The numerical resolution of parabolic PDEs demands significant computational effort, and the Monte Carlo method requires solving the model several times. For these reasons, computational execution time becomes an issue. To obtain the simulations results faster, the present study employs a computational parallelization strategy for shared memory architectures using the *OpenMP* Application Programming Interface (API).

We organise this paper as follows. Section 2 describes the bioheat model, numerical approximation and the uncertainty quantification. The results are presented in section 3 and discussed in section 4. Finally, section 5 presents the conclusions and plans for future work.

2 Methods

2.1 Mathematical Model

A porous medium is a material consisting of a solid matrix with an interconnected void [13]. The biological tissues can be seen as a porous medium once they contain dispersed cells separated by voids that allow the flow of nutrients, minerals, and others to reach all cells within the tissue. A fundamental characteristic of this medium is its porosity (ε), defined as the ratio of the void space to the local volume of the medium, and also by its permeability which is a measure of the flow conductivity in this medium.

Heat transfer in human tissues involves complicated processes such as heat conduction in tissues, heat transfer due to blood convection, metabolic heat generation, and others [13]. The dynamics of heat in living tissue is called bioheat. Many scientists have attempted to model bioheat accurately since it is the basis for the human thermoregulation system [30] as well as thermotherapies [31]. The bioheat equation usually expresses the energy transport in a biological system, and the one developed by Pennes [21] is among the earliest models for bioheat.

The application of porous media models for modeling bioheat transfer in human tissues is relatively recent. Xuan and Roetzel [26, 35] used the concepts of transport through porous media to model the tissue-blood system composed mainly of tissue cells (solid particles) and interconnected voids that contain arterial or venous blood. They adopted the idea of a local thermal non-equilibrium model as described in the works of Amiri and Vafai [2, 3], Alazmi and Vafai [1], and Lee and Vafai [14] to model heat transfer within the tissue and the artery blood. However, Xuan and Roetzel [26, 35] indicated that numerous parameters and information are needed to solve the system, which consists of a two-phase energy equation, such as thermal and anatomic properties of the tissue, interstitial convective heat transfer coefficients as well as the velocity field of the blood [13].

ICCS Camera Ready Version 2023
To cite this paper please use the final published version:
DOI: 10.1007/978-3-031-36021-3_60

Local thermal equilibrium can be used as a good approximation for the temperature field in specific applications with capillaries bed, as shown in the literature [1–3, 14]. In this case, blood and tissue temperatures are the same at any location, according to the following equation:

$$[\rho c_p(1-\varepsilon)+\rho_b c_{p_b}\varepsilon]\frac{\partial T}{\partial t}+\varepsilon(\rho c_p)_b\mathbf{u}_b\cdot\nabla T=\nabla\left([\mathbf{k}_s^a+\mathbf{k}_b^a]\cdot\nabla T\right)+Q_m(1-\varepsilon), \quad (1)$$

where T, ρ, ρ_b, c_p, ε, c_{p_b}, $\mathbf{u}_b$, $\mathbf{k}_s^a$, $\mathbf{k}_b^a$, Q_m are the tissue (and the blood) temperature, the tissue density, the blood density, the specific heat of tissue, the porosity of the tissue, the specific heat of blood, blood velocity field, tissue effective thermal conductivity tensor, blood effective thermal conductivity tensor, and heat generation within the tissue, respectively. Once we are considering an isotropic conduction, $\mathbf{k}_b^a=(1-\varepsilon)k_t$, $\mathbf{k}_b^a=\varepsilon k_b$, k_t and k_b are the tissue and blood thermal conductivities, respectively.

However, modeling the heat generated by the magnetic nanoparticles is necessary. An *in vivo* experimental study done by Salloum [29] and performed on hindlimbs of rats showed that the specific absorption rate (SAR) around an injection site can be approximated by:

$$Q_r(\vec{x})=\sum_{i=1}^{M}A_i e^{\frac{-r_i^2}{r_{0,i}^2}}, \quad (2)$$

where M is the number of nanoparticle injections into the tumor, A is the maximum heat generation rate, r is the distance to the injection point, and r_0 is the hyperthermia coverage radius. Adding this term to Equation (1), in a well-posed problem, proper boundary conditions on a Lipschitz continuous, and piecewise smooth boundary and initial conditions, the model is given as follows:

$$\begin{cases}\sigma\dfrac{\partial T}{\partial t}+\varepsilon(\rho c_p)_b\mathbf{u}_b\cdot\nabla T=\nabla\left(\kappa\cdot\nabla T\right)+(1-\varepsilon)\left(Q_m+Q_r\right) & \text{in } \Omega\times I,\\ T(.,0)=37 & \text{on } \partial\Omega\times I,\\ \kappa\nabla T\cdot\vec{n}=0 & \text{in } \Omega,\end{cases} \quad (3)$$

where $\Omega\subset\mathbb{R}^2$ is the spatial domain, $I\subset\mathbb{R}^+$ is the time domain, $T:\Omega\times I\to\mathbb{R}^+$ is the temperature, $\sigma=[\rho c_p(1-\varepsilon)+\rho_b c_{pb}\varepsilon]$, $\kappa=(1-\epsilon)k_t+\epsilon k_b$.

2.2 Numerical Scheme

The numerical method used to solve Equation (3) is the Finite Difference Method (FDM). We consider a heterogeneous medium and the closed domain Ω discretized into a set of regular points defined by $S_\Omega=\{(x_i,y_j);i=0,1,\cdots,N_x;j=0,1,\cdots,N_y\}$, where $N_x=N_y=N$ is the number of intervals of length $h_x=h_y=h$. Moreover, the time discretization of the time domain I is partitioned into N_t equal time intervals of length h_t, *i.e.*, $S_I=\{(t_n);n=0,1,\cdots,N_t\}$. To obtain the discrete form of the model, we employ an FTCS scheme, resulting in

ICCS Camera Ready Version 2023
To cite this paper please use the final published version:
DOI: 10.1007/978-3-031-36021-3_60

an explicit numerical method. Moreover, we use a first-order upwind scheme to the advection term [15]:

$$T_{i,j}^{n+1} = \frac{h_t}{\sigma}\left(\varphi_{dif}(T^n) - \varphi_{adv}(T^n) + (1-\varepsilon)Q_m + Q_r\right) + T_{i,j}^n, \tag{4}$$

where

$$\begin{aligned}\varphi_{dif}(T^n) = &\frac{\kappa_{i+1/2,j}(T_{i+1,j,k}^n - T_{i,j}^n) - \kappa_{i-1/2,j}(T_{i,j}^n - T_{i-1,j}^n)}{h^2} + \\ &\frac{\kappa_{i,j+1/2}(T_{i,j+1}^n - T_{i,j}^n) - \kappa_{i,j-1/2}(T_{i,j}^n - T_{i,j-1,k}^n)}{h^2},\end{aligned} \tag{5}$$

where $\kappa_{i+1/2,j,k}$ is the thermal conductivity evaluated at the midpoint. In this paper we consider a piecewise homogeneous media where the thermal conductivity is a discontinuous function, so the thermal conductivity can be estimated using the harmonic mean, *i.e.*:

$$\kappa_{i+1/2,j} \approx \frac{2\kappa_{i,j}\kappa_{i+1,j}}{\kappa_{i,j} + \kappa_{i+1,j}}. \tag{6}$$

Equation (6) assures the continuity of the flux. Furthermore, the thermal conductivity for the other midpoints is evaluated using the same idea.

Furthermore,

$$\varphi_{adv}(T^n) = \varepsilon(\rho c_p)_b \mathbf{u}_{b_{i,j}} \cdot \begin{pmatrix} \begin{cases} \dfrac{(u_{i,j}^n - u_{i-1,j}^n)}{h} & \text{for } u_{b_x} > 0 \\ \dfrac{(u_{i+1,j}^n - u_{i,j}^n)}{h} & \text{for } u_{b_x} < 0 \end{cases} \\ \begin{cases} \dfrac{(u_{i,j}^n - u_{i,j-1}^n)}{h} & \text{for } u_{b_y} > 0 \\ \dfrac{(u_{i,j+1}^n - u_{i,j}^n)}{h} & \text{for } u_{b_y} < 0 \end{cases} \end{pmatrix} \tag{7}$$

where $\mathbf{u}_b = \begin{pmatrix} u_{b_x} \\ u_{b_y} \end{pmatrix}$.

2.3 Uncertainty Quantification

We employ the Monte Carlo method to quantify two uncertainty scenarios [28]: a) the influence of the capillaries architecture and b) the influence of the blood velocity. The first scenario was divided in two, one considering only the influence of the number of capillaries terminals and the other considering only the influence of the angle of capillaries terminals.

We consider the terminal points of the capillary bed uniformly distributed in the domain for all scenarios. Once cancer growth can stimulate the capillaries'

ICCS Camera Ready Version 2023
To cite this paper please use the final published version:
DOI: 10.1007/978-3-031-36021-3_60

angiogenesis in the tumor site [8, 37], we consider the tumor tissue with 70% of capillaries terminals and the healthy tissue with 50% of capillaries terminals as the base values. Furthermore, the blood velocity also depends on the cancer type, stage, location, and other specificities [11, 37]. So we consider the magnitude of the blood velocity as 3mm/s in the tumor tissue and 2mm/s in the healthy tissue as the base values. Finally, we draw the angle for each terminal point using values uniformly distributed between 0 and 2π.

For the first scenario, the influence of the number of capillaries, we drew all terminal points and angles for the entire tissue. For each MC simulation, we use the following expression to determine the number of capillaries:

$$N_c = \begin{cases} 70 \times X \sim U(0.7, 1.3) & \text{for the tumor tissue,} \\ 50 \times X \sim U(0.7, 1.3) & \text{otherwise,} \end{cases}$$

where N_c is the percentage of capillaries terminals in the respective tissue and $X \sim U(a, b)$ is a uniform distribution that generates a random value between a and b.

In the second part of the first scenario, the influence of the capillaries angles, we drew terminal points and base angles (using the proportion of 50% to healthy tissue and 70% to the tumor one). For each MC simulation, we use the following expression to determine the angle of capillaries:

$$\theta_c = \theta \times X \sim U(0.7, 1.3),$$

where θ is the base angle of the capillary and θ_c is the value considering the uncertainties of 30% in the capillary angles.

In the second scenario, the influence of the blood velocity magnitude, we drew terminal points and base angles (using the proportion of 50% to healthy tissue and 70% to the tumor one). We consider 50% of the uncertainty in the magnitude for each MC sample using the following expression:

$$|\mathbf{u_{b_c}}| = |\mathbf{u_b}| \times X \sim U(0.5, 1.5),$$

where $|\mathbf{u_b}|$ is the magnitude of blood velocity (see Table 1) and $|\mathbf{u_{b_c}}|$ is the value considering the uncertainty.

Finally, the Algorithm 1 illustrates the implementation of uncertainty quantification via Monte Carlo using *OpenMP* used in this study. It is worthwhile to notice that `omp parallel` command creates the threads and `omp for` divides the workload among the created threads. Moreover, the time loop has no workload division once data dependence exists between successive time steps.

3 Numerical Results

This section presents the results of the two scenarios evaluated in this work. Both simulation scenarios consider a two-dimensional domain with the tissue consisting only of healthy and tumor cells. The healthy cells represent a piece of

ICCS Camera Ready Version 2023
To cite this paper please use the final published version:
DOI: 10.1007/978-3-031-36021-3_60

Algorithm 1: Pseudocode of Monte Carlo implementation using *OpenMP*

```
begin
    # pragma omp parallel
    foreach Monte Carlo Sample do
        foreach t_n; n = 0, 1, ..., N_t do
            #pragma omp for
            foreach (x_i, y_j); i = 0, 1, ..., N_x; j = 0, 1, ..., N_y do
                evaluate T_ij^{n+1} using Equation (4)
            end
        end
    end
end
```

muscle tissue. Also, we performed 10,000 MC simulations of cancer treatment with hyperthermia using magnetic nanoparticles, considering a square domain of length $0.1m$ and a tumor seated in $(x, y) \in [0.04, 0.06] \times [0.04, 0.06]$. The model parameters used for solving Equation 3 are specified in Table 1. Furthermore, we consider a single nanoparticles injection point seated at $(0.50m, 0.50m)$.

Table 1. Model parameters values employed in Equation (3).

Symbol	Unit	Muscle	Tumor
c	$(J/Kg°C)$	4,000	4,000
c_{pb}	$(J/Kg°C)$	4,000	4,000
k	$(W/m°C)$	0.50	0.55
p	(Kg/m^3)	1,000	1,200
ρ_b	(Kg/m^3)	1,000	1,000
ε	-	0.02	0.01
q_m	(W/m^3)	420	4,200
$\lvert\mathbf{u}_b\rvert$	(mm/s)	2.0	3.0
A	W/m^3	0.9×10^6	
r_0	m	3.1×10^{-3}	

The numerical model presented in Section 2 was implemented using the C++ programming language and the *OpenMP* API. The code was compiled using *gcc* version 11.3.1 with the optimization flag $-O3$ enabled. The code was executed in a 2.90 GHz Intel® Core™ *i*7-10700 CPU. Although this CPU has 16 hyperthreading cores, the number of physical cores available is 8, which is the number of threads used during simulations. Finally, the post-processing of the simulations was performed using `matplotlib` library [10] and *ParaView* version 5.10.1 [4].

ICCS Camera Ready Version 2023
To cite this paper please use the final published version:
DOI: 10.1007/978-3-031-36021-3_60

3.1 Influence of the capillaries architecture

The uncertainty quantification simulation results considering the influence of the capillary bed architecture are divided into two scenarios, presented in the following subsections.

The number of capillaries Figure 1A shows the base distribution of the velocity field for the capillary bed considering the uncertainties described in Section 2.3, *i.e.*, considering 30% of uncertainty in the number of capillaries terminals.

Figure 1B shows the average temperature obtained after 10,000 MC simulations at $t = 50min$. It is worth noting that the white isoline of 43^oC covers the entire tumor (the solid black line), *i.e.*, the tumor tissue reaches the target temperature that causes necrosis.

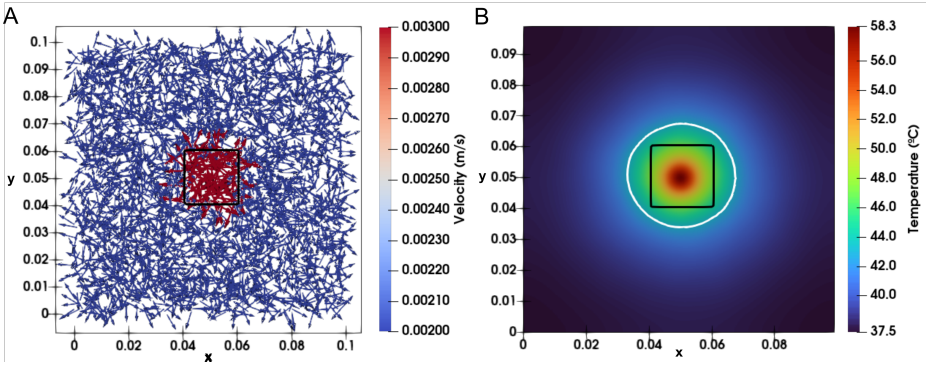

Fig. 1. Simulation of the number of capillaries' influence in the hyperthermia treatment. **A)** Base velocity field considering 100% of capillaries; **B)** Average temperature distribution for 10,000 Monte Carlo simulations at $t = 50min$ employing Equation (4) with a tumor located in $(x, y) \in [0.04, 0.06] \times [0.04, 0.06]$ and considering the parameters present in Table 1. The solid white contour represents the temperature of 43^oC, highlighting the damaged area, and the solid black contour is the tumor tissue location.

Figure 2A presents the evolution of the average temperature of the tumor tissue and healthy tissue. It is worthwhile to notice that the temperature inside the tumor is higher than that of the healthy portion. Moreover, even considering the 95% confidence interval (CI), the average temperature of the tumor is higher than 43^oC. On the other hand, Figure 2B shows that only 5.2% of the healthy tissue reached a temperature of 43^oC or higher while the tumor tissue reached the target temperature with a mean value close to the 95% CI limits.

Angles of capillaries This section presents the simulation results obtained after using the uncertainties described in Section 2.3 for analyzing the influence

ICCS Camera Ready Version 2023
To cite this paper please use the final published version:
DOI: 10.1007/978-3-031-36021-3_60

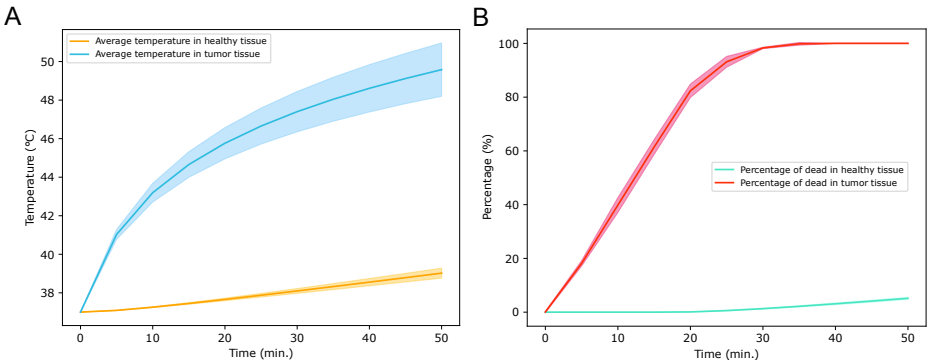

Fig. 2. Uncertainty quantification of the influence of the number of capillaries in the hyperthermia treatment. In both figures, the solid lines represent the mean temperature, and shade regions represent the 95% confidence interval obtained after 10,000 Monte Carlo simulations. **A)** Evolution of temperature obtained by Eq. (4) considering the parameters present in Table 1. The blue line and blue shade represent the average temperature of the tumor, and the yellow line and yellow shade represent the average temperature of healthy tissue; **B)** Percentage of tumor and healthy tissues killed by hyperthermia. The red line and red shaded represent tumor tissue necrosis, and the green line and green shade represent healthy tissue necrosis.

of the capillary terminals' angles, *i.e.*, considering 30% of uncertainty in the capillary terminals' angles. Figure 3A shows the base distribution of the velocity field of the capillary bed, considering 70% of blood vessels in cancerous tissue and 50% in healthy tissue.

Figure 3B shows the average temperature obtained after 10,000 MC simulations at $t = 50min$. The tumor reaches the target temperature that causes necrosis once the white isoline of 43^oC covers the entire tumor (the solid black line).

Figure 4A presents the evolution of the average tumor and healthy tissues temperature. Again, the temperature inside the tumor is higher than that of the healthy portion. Moreover, even considering the 95% confidence interval, the average temperature of the tumor tissue is higher than 43^oC. On the other hand, Figure 4B shows that only 5.3% of healthy tissue reached a temperature of 43^oC or higher while the tumor tissue reached the target temperature with 95% CI in $[99.5, 100]$.

3.2 Influence of the blood velocity

This section presents the simulation results obtained after using the uncertainties described in Section 2.3 for the analysis of the blood velocity magnitude influence, *i.e.*, considering 50% of uncertainty in the magnitude of the blood velocity. Figure 5A shows the base distribution of the velocity field of the capillary bed considering 70% of blood vessels in cancerous tissue and 50% in healthy tissue as well as the blood velocity given by Table 1.

ICCS Camera Ready Version 2023
To cite this paper please use the final published version:
DOI: 10.1007/978-3-031-36021-3_60

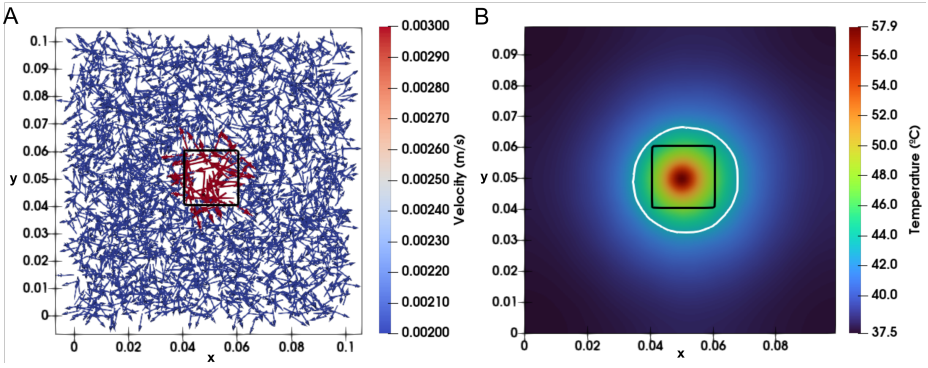

Fig. 3. Simulation of the influence of the capillaries angles in the hyperthermia treatment. **A)** Base velocity field considering 70% of capillaries in the tumor tissue and 50% of capillaries in the healthy tissue; **B)** Average temperature distribution obtained after 10,000 Monte Carlo simulations at $t = 50min$ employing Equation (4) with a tumor located in $(x, y) \in [0.04, 0.06] \times [0.04, 0.06]$ and considering the parameters present in Table 1. The solid white contour represents the temperature of 43^oC, highlighting the damaged area, and the solid black contour is the tumor location.

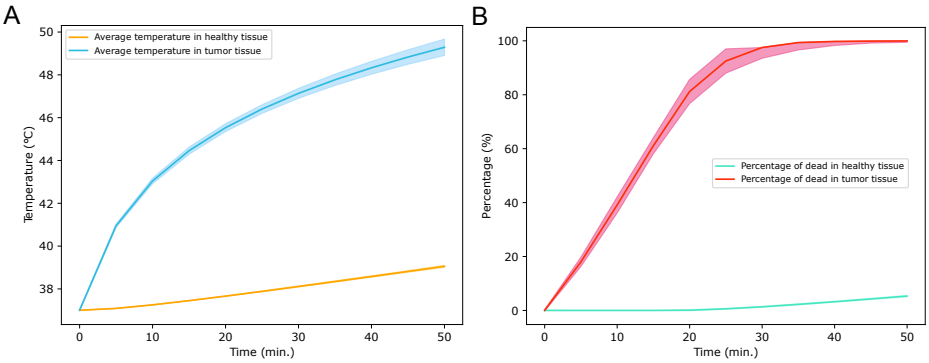

Fig. 4. Uncertainty quantification of the influence of the capillaries angles in the hyperthermia treatment. In both figures, the solid lines represent the mean temperature, and shade regions represent the 95% confidence interval for 10,000 Monte Carlo simulations. **A)** Evolution of temperature determined by Eq. (4) considering the parameters present in Table 1. The blue line and blue shade represent the average temperature of the tumor, and the yellow line and yellow shade represent the average temperature of healthy tissue; **B)** Percentage of tumor and healthy tissues killed by hyperthermia. The red line and red shaded represent tumor tissue necrosis, and the green line and green shade represent healthy tissue necrosis.

Figure 5B shows the average temperature obtained after 10,000 MC simulations at $t = 50min$. The tumor tissue reaches the target temperature that causes necrosis once the white isoline of 43^oC covers the entire tumor (the solid black line).

ICCS Camera Ready Version 2023
To cite this paper please use the final published version:
DOI: 10.1007/978-3-031-36021-3_60

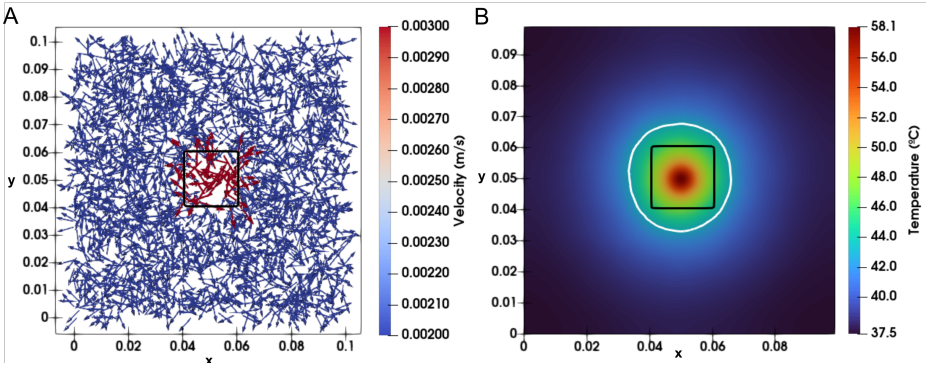

Fig. 5. Simulation of the influence of the blood velocity magnitude in the hyperthermia treatment. **A)** Base velocity field considering 70% of capillaries in the tumor tissue and 50% of capillaries in the healthy tissue; **B)** Average temperature distribution obtained after 10,000 Monte Carlo simulations at $t = 50min$ employing Equation (4) with a tumor located in $(x, y) \in [0.04, 0.06] \times [0.04, 0.06]$ and considering the parameters present in Table 1. The solid white contour represents the temperature of 43^oC, highlighting the damaged area, and the solid black contour is the tumor location.

Figure 6A presents the evolution of the average temperature for the tumor and the healthy tissue. As in the previous scenario, the temperature inside the tumor tissue is higher than that of the healthy portion. Moreover, even considering the 95% confidence interval, the average temperature of the tumor is higher than 43^oC. Figure 6B shows that only 5.1% of healthy tissue reached a temperature of 43^oC or higher while the tumor tissue reached the target temperature with a mean value close to the 95% CI limits.

4 Discussion

Considering the influence of the capillary bed architecture and blood velocity magnitude from the numerical results presented in Section 3, it is possible to assume that, in all cases, the average temperature value in the tumor site rises above 43^oC, which leads to its damage. Moreover, in all scenarios, the health tissue damage was less than 6%. Figures 2, 4, and 6 demonstrate that the entire tumor reaches the target temperature when considering the average value. Even when the limits of the CI are considered, the hyperthermia treatment damages the entire tumor site, except in the case illustrated in Figure 4.

Figures 1, 3, and 5 show that the number of capillaries is the variable analyzed in this work that adds more uncertainty to the model results, impacting especially the tumor tissue temperature. The capillary angles and the blood velocity seem to add small amounts of uncertainties to the model resolution, especially to the computation of damage to healthy tissue. These results indicate that a good representation of capillaries may be essential to obtain realistic simulations

ICCS Camera Ready Version 2023
To cite this paper please use the final published version:
DOI: 10.1007/978-3-031-36021-3_60

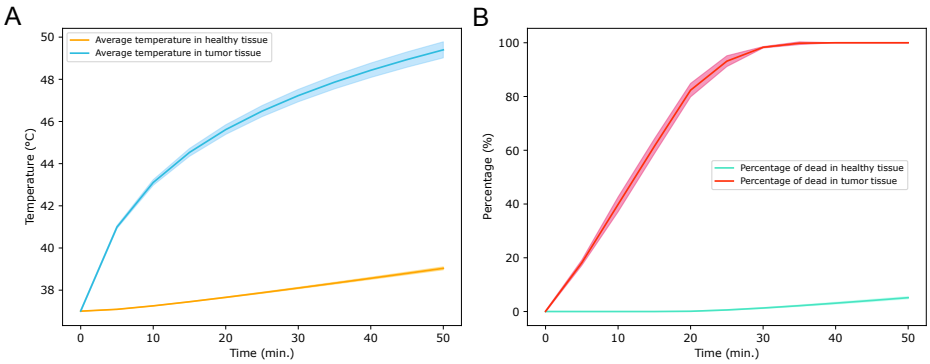

Fig. 6. Uncertainty quantification of the influence of the blood velocity magnitude in the hyperthermia treatment. In both figures, the solid lines represent the mean temperature, and shade regions represent the 95% confidence interval for 10,000 Monte Carlo simulations. **A)** Evolution of temperature determined by the Eq. (4) considering the parameters present in Table 1. The blue line and blue shade represent the average temperature of the tumor, and the yellow line and yellow shade represent the average temperature of healthy tissue; **B)** Percentage of tumor and healthy tissue killed by hyperthermia. The red line and red shaded represent tumor tissue necrosis, and the green line and green shade represent healthy tissue necrosis.

of the hyperthermia treatment results or, from a medical perspective, should be taken into account in the treatment.

It is essential to notice the limitations of this study. For example, this paper establishes a temperature threshold of $T \geq 43^oC$ for inducing tissue damage and cell necrosis. But this threshold is considered a threshold temperature to cause cell necrosis within a reasonable duration. During our experiments, we simulated 50 minutes of hyperthermia treatment but did not consider the duration as a parameter for determining hyperthermia success. Also, there is a delay in achieving tissue damage at this temperature, which is not considered in this paper. Additionally, there exist more accurate methods for measuring tumor ablation, such as the Arrhenius models [32, 33]. Lastly, it is important to acknowledge that this study relies on a theoretical model and may not entirely reflect the intricate biological processes that occur in actual tumors. Furthermore, the outcomes of this research may not be immediately applicable to clinical environments, and additional experimental verification is necessary.

5 Conclusions and Future Works

This work presents the results of a two-dimensional simulation of hyperthermia cancer treatment in a heterogeneous porous tissue and UQ analysis via Monte Carlo simulation. The results presented in this study suggest that the capillaries bed architecture significantly influences temperature evolution in the simulated tissue. On the other hand, the target temperature of 43^oC at the final of the

ICCS Camera Ready Version 2023
To cite this paper please use the final published version:
DOI: 10.1007/978-3-031-36021-3_60

treatment presents little influence under the assumption of these uncertainties when considering the parameters used to perform these simulations. This study demonstrates that uncertainty analysis can be a powerful tool for treatment planning once it allows the possibility to perform several *in silico* trials and analyze the best option for a patient-specific scenario, taking into account the experimental uncertainties such as limited accuracy of the measuring apparatus, limitations and simplifications of the experimental procedure and uncontrolled changes to the environment. The results of this paper reinforce that *in silico* medicine might reduce the need for clinical trials with animals and cohort studies with humans.

Although this paper aims to analyze the uncertainty introduced by the values associated with the capillaries bed architecture and the magnitude of the blood velocity parameters in the results of the mathematical model, using a simple approach for this purpose, it is possible to employ different types of probability density functions, for example, fitted from experimental data. Additional studies are needed to determine the uncertain parameters' best probability density function. In addition, the uncertainties introduced by other parameters can be included in the analysis to determine their impact on the results of the mathematical model simulation. Furthermore, it is also essential to consider the study of different tissue layers in the human body, such as skin, muscle, and fat, along with realistic tumor and tissue shapes. Furthermore, we intend to assess the suggested approach on more practical tumors and diverse tissue shapes or even use tumors derived from images specific to a patient as demonstrated in studies available in the literature [22, 23, 36].

Acknowledgments

The authors would like to express their thanks to CAPES (Finance Code 001 and Projeto CAPES - Processo 88881.708850/2022-01), CNPq (308745/2021-3), FAPEMIG (APQ-02830/17 and APQ-01226-21), FINEP (SOS Equipamentos 2021 AV02 0062/22) and UFJF for funding this work.

References

1. Alazmi, B., Vafai, K.: Constant wall heat flux boundary conditions in porous media under local thermal non-equilibrium conditions. International Journal of Heat and Mass Transfer **45**(15), 3071–3087 (2002)
2. Amiri, A., Vafai, K.: Transient analysis of incompressible flow through a packed bed. International Journal of Heat and Mass Transfer **41**(24), 4259–4279 (1998)
3. Amiri, A., Vafai, K.: Analysis of dispersion effects and non-thermal equilibrium, non-darcian, variable porosity incompressible flow through porous media. International journal of heat and mass transfer **37**(6), 939–954 (1994)
4. Ayachit, U.: The paraview guide: a parallel visualization application. Kitware, Inc. (2015)

ICCS Camera Ready Version 2023
To cite this paper please use the final published version:
DOI: 10.1007/978-3-031-36021-3_60

5. Gilchrist, R.K., Medal, R., Shorey, W.D., Hanselman, R.C., Parrott, J.C., Taylor, C.B.: Selective inductive heating of lymph nodes. Annals of Surgery **146**(4), 596–606 (1957)
6. Giustini, A.J., Petryk, A.A., Cassim, S.M., Tate, J.A., Baker, I., Hoopes, P.J.: Magnetic nanoparticle hyperthermia in cancer treatment. Nano Life **1**(01n02), 17–32 (2010). https://doi.org/10.1142/S1793984410000067
7. Guedes, B.R., Lobosco, M., dos Santos, R.W., Reis, R.F.: Uncertainty quantification of tissue damage due to blood velocity in hyperthermia cancer treatments. In: Computational Science–ICCS 2021: 21st International Conference, Krakow, Poland, June 16–18, 2021, Proceedings, Part II 21. pp. 511–524. Springer (2021)
8. Hicklin, D.J., Ellis, L.M.: Role of the vascular endothelial growth factor pathway in tumor growth and angiogenesis. Journal of clinical oncology **23**(5), 1011–1027 (2005)
9. Hilger, I., Hergt, R., Kaiser, W.A.: Towards breast cancer treatment by magnetic heating. Journal of Magnetism and Magnetic Materials **293**(1), 314 – 319 (2005), proceedings of the Fifth International Conference on Scientific and Clinical Aplli-cations of Magnetic Carriers
10. Hunter, J.D.: Matplotlib: A 2d graphics environment. Computing in Science & Engineering **9**(3), 90–95 (2007). https://doi.org/10.1109/MCSE.2007.55
11. Ishida, H., Hachiga, T., Andoh, T., Akiguchi, S.: In-vivo visualization of melanoma tumor microvessels and blood flow velocity changes accompanying tumor growth. Journal of Applied Physics **112**(10), 104703 (2012)
12. Jiji, L.M.: Heat Conduction. Springer-Verlag Berlin Heidelberg (2009)
13. Khaled, A.R., Vafai, K.: The role of porous media in modeling flow and heat transfer in biological tissues. International Journal of Heat and Mass Transfer **46**(26), 4989 – 5003 (2003)
14. Lee, D.Y., Vafai, K.: Analytical characterization and conceptual assessment of solid and fluid temperature differentials in porous media. International Journal of Heat and Mass Transfer **42**(3), 423–435 (1999)
15. LeVeque, R.J.: Finite difference methods for ordinary and partial differential equations: steady-state and time-dependent problems. SIAM (2007)
16. Matsuki, H., Yanada, T., Sato, T., Murakami, K., Minakawa, S.: Temperature-sensitive amorphous magnetic flakes for intratissue hyperthermia. Materials Science and Engineering: A **181**(0), 1366 – 1368 (1994), proceedings of the Eighth International Conference on Rapidly Quenched and Metastable Materials: Part 2
17. Minkowycz, W., Sparrow, E.M., Abraham, J.P.: Nanoparticle heat transfer and fluid flow, vol. 4. CRC press (2012)
18. Moros, E.: Physics of thermal therapy: fundamentals and clinical applications. CRC Press (2012)
19. Moroz, P., Jones, S., Gray, B.: Magnetically mediated hyperthermia: current status and future directions. International Journal of Hyperthermia **18**(4), 267–284 (2002)
20. National Cancer Institute: Types of cancer treatment. `https://www.who.int/health-topics/cancer`. Last accessed 1 March 2023 (2023)
21. Pennes, H.H.: Analysis of tissue and arterial blood temperature in the restind human forearm. Journal of Applied Phisiology **1**, 93–122 (1948)
22. Prasad, B., Ha, Y.H., Lee, S.K., Kim, J.K.: Patient-specific simulation for selective liver tumor treatment with noninvasive radiofrequency hyperthermia. Journal of Mechanical Science and Technology **30**, 5837–5845 (2016)
23. Rahpeima, R., Lin, C.A.: Numerical study of magnetic hyperthermia ablation of breast tumor on an anatomically realistic breast phantom. Plos one **17**(9), e0274801 (2022)

ICCS Camera Ready Version 2023
To cite this paper please use the final published version:
DOI: 10.1007/978-3-031-36021-3_60

24. Reis, R.F., dos Santos Loureiro, F., Lobosco, M.: Parameters analysis of a porous medium model for treatment with hyperthermia using openmp. Journal of Physics: Conference Series **633**(1), 012087 (2015)
25. Reis, R.F., dos Santos Loureiro, F., Lobosco, M.: 3d numerical simulations on gpus of hyperthermia with nanoparticles by a nonlinear bioheat model. Journal of Computational and Applied Mathematics **295**, 35–47 (2016)
26. Roetzel, W., Xuan, Y.: Transient response of the human limb to an external stimulust. International journal of heat and mass transfer **41**(1), 229–239 (1998)
27. Rosensweig, R.: Heating magnetic fluid with alternating magnetic field. Journal of Magnetism and Magnetic Materials **252**(0), 370 – 374 (2002), proceedings of the 9th International Conference on Magnetic Fluids
28. Rubinstein, R.Y., Kroese, D.P.: Simulation and the Monte Carlo method. John Wiley & Sons (2016)
29. Salloum, M., Ma, R., Zhu, L.: An in-vivo experimental study of temperature elevations in animal tissue during magnetic nanoparticle hyperthermia. International Journal of Hyperthermia **24**(7), 589–601 (2008)
30. Sanyal, D., Maji, N.: Thermoregulation through skin under variable atmospheric and physiological conditions. Journal of Theoretical Biology **208**(4), 451–456 (2001)
31. Sherar, M.D., Gladman, A.S., Davidson, S.R., Trachtenberg, J., Gertner, M.R.: Helical antenna arrays for interstitial microwave thermal therapy for prostate cancer: tissue phantom testing and simulations for treatment. Physics in Medicine & Biology **46**(7), 1905 (2001)
32. Singh, M.: Incorporating vascular-stasis based blood perfusion to evaluate the thermal signatures of cell-death using modified arrhenius equation with regeneration of living tissues during nanoparticle-assisted thermal therapy. International Communications in Heat and Mass Transfer **135**, 106046 (2022). https://doi.org/10.1016/j.icheatmasstransfer.2022.106046
33. Singh, M., Singh, T., Soni, S.: Pre-operative assessment of ablation margins for variable blood perfusion metrics in a magnetic resonance imaging based complex breast tumour anatomy: simulation paradigms in thermal therapies. Computer Methods and Programs in Biomedicine **198**, 105781 (2021). https://doi.org/10.1016/j.cmpb.2020.105781
34. WHO: World health organization. `https://www.who.int/news-room/fact-sheets/detail/cancer`. Last accessed 23 March 2023 (2023)
35. Xuan, Y., Roetzel, W.: Bioheat equation of the human thermal system. Chemical Engineering & Technology: Industrial Chemistry-Plant Equipment-Process Engineering-Biotechnology **20**(4), 268–276 (1997)
36. Zastrow, E., Hagness, S.C., Van Veen, B.D.: 3d computational study of non-invasive patient-specific microwave hyperthermia treatment of breast cancer. Physics in Medicine & Biology **55**(13), 3611 (2010)
37. Zhou, W., Chen, Z., Zhou, Q., Xing, D.: Optical biopsy of melanoma and basal cell carcinoma progression by noncontact photoacoustic and optical coherence tomography: In vivo multi-parametric characterizing tumor microenvironment. IEEE transactions on medical imaging **39**(6), 1967–1974 (2019)

ICCS Camera Ready Version 2023
To cite this paper please use the final published version:
DOI: 10.1007/978-3-031-36021-3_60